# **Integrated Photonic Slow Light Michelson Interferometer Bio Sensor**

Jianhao Shen, Daniel Donnelly, Swapnajit Chakravarty
Department of Electro-Optics and Photonics, University of Dayton, 300 College Park, Dayton, OH
USA 45469

#### **ABSTRACT**

Diverse chip-based sensors utilizing integrated silicon photonics have been demonstrated in resonator and phase shifter/interferometer configurations. Till date, interferometric techniques with the Mach-Zehnder Interferometer (MZI) and Young's interferometer have shown the lowest mass detection limits (in pg/mm²). Slow light in photonic crystal waveguides integrated with MZIs enables compact geometries due to enhanced optical path lengths as light propagates with high group index. In a typical MZI, light propagating in the signal arm overlaps with analytes and undergo a relative phase change with respect to the light in the reference arm which leads to measured output intensity changes. In this paper, using integrated photonic methods, we demonstrate a slow light enhanced Michelson interferometer (MI) biosensor, wherein the reference and signal arms are traversed twice by the propagating optical mode. As a result, the analyte interaction length is effectively doubled since the propagating optical mode undergoes twice the phase shift as would be observed in a MZI. In an asymmetric MI configuration, the resultant doubling of the phase shift is observed as a doubling of the resonance wavelength shift for a fixed change in the analyte concentration. The device sensitivity is thus doubled with respect to a conventional MZI while also effectively halving the geometric length compared to the MZI sensor.

Keywords: Photonic crystal, slow light, interferometer, Mach-Zehnder, Michelson, biosensor, silicon photonics

#### 1. INTRODUCTION

With the advancement of silicon integrated photonics for on-chip computing and on-chip signal modulation and routing for optical transceiver applications, a parallel application in label-free photonic biosensing has been extensively studied over the past decade [1-8]. The applications for photonic biosensing are numerous, ranging from the detection of cancers [7] and infectious diseases to the monitoring of environmental pollutants in water [8]. Similar to their microarray fluorescent labeled counterparts, label-free silicon photonic biosensing also requires many sensors to be integrated on a silicon chip to enable a measurement of signal and control biomarker conjugate binding responses not only with high sensitivity and specificity but also with repeatability across several similarly receptor functionalized cavities to build confidence in the measurements. The small dimensions of microring resonator (MRR) cavities with typical diameters ~10microns, or photonic crystal (PC) type nanocavities, with typical cavity dimensions ~1-2 microns, ensures of course that several resonator cavities can be packed into a narrow microfluidic channel. As a result, chip integrated silicon photonic biosensor platforms require few tens of micro-liters of the analyte sample in contrast to much larger milli-liter volumes in standard fluorescent microarray applications.

The nanocavity resonators (both the MRR and PC type) show a limiting sensitivity ~10<sup>-6</sup>/RIU (RIU=refractive index unit). In contrast, Mach-Zehnder Interferometer (MZI) type biosensors on the silicon photonic platform have a limiting sensitivity ~10<sup>-7</sup>/RIU which make them more attractive for high sensitivity sensing [9]. However, the Mach-Zehnder type devices are typically a few hundred microns long which consequently results in fewer number of functionalized MZI-type sensors that can be multiplexed in the same chip area. In this paper, we investigate two approaches to reduce the interferometer dimensions, first by implementing a Michelson Interferometer (MI) to half the required MZI geometric length, and second by implementing slow light photonic crystal-based interferometry that scales the length down in proportion to the slow wave group index.

### 2. DESIGN

### 2.1 Michelson Interferometry On-Chip

Fig. 1(a) shows a typical schematic of a MZI on a silicon photonic chip. A  $1\times2$  MMI (multimode interferometer) splits the input light into two parallel arms. In the asymmetric MZI, the physical path length on the two arms differs by a length  $\Delta L$ . When the two asymmetric arms are combined by another  $2\times1$  MMI, the output of the  $2\times1$  MMI combiner shows

<sup>\*</sup>schakravarty1@udayton.edu; phone 1 937 229-2747;

interference fringes with a free spectral range (FSR) determined by the phase difference ( $\Delta \phi$ ) between the two arms given by:

$$\Delta \phi = k_0 n_{eff} \Delta L$$

Where  $n_{eff}$  is the effective index of the propagating optical mode, and  $k_0=2\pi/\lambda$  is the wavevector at wavelength ( $\lambda$ ). When the two arms of the interferometer are terminated by a loop mirror with a 1×2 MMI, the output of the 1×2 MMI are reflected back to the asymmetric arms as in an Michelson Interferometer shown schematically in Fig. 1(b), thereby effectively doubling  $\Delta L$  and hence doubling the corresponding phase shift to  $2\times\Delta\varphi$ . The resultant effect is observed in the interference fringes at the output. As seen in Fig. 1(c), the interference fringe spacing is halved in the MI for the same geometric path length as in a MZI. Interference fringes in the MI also have a higher quality factor than the MZI due to the doubled path length difference, which would thus enable the measurement of smaller refractive interference changes due to the corresponding shift in the interference fringe in wavelength as observed in Fig. 1(d).

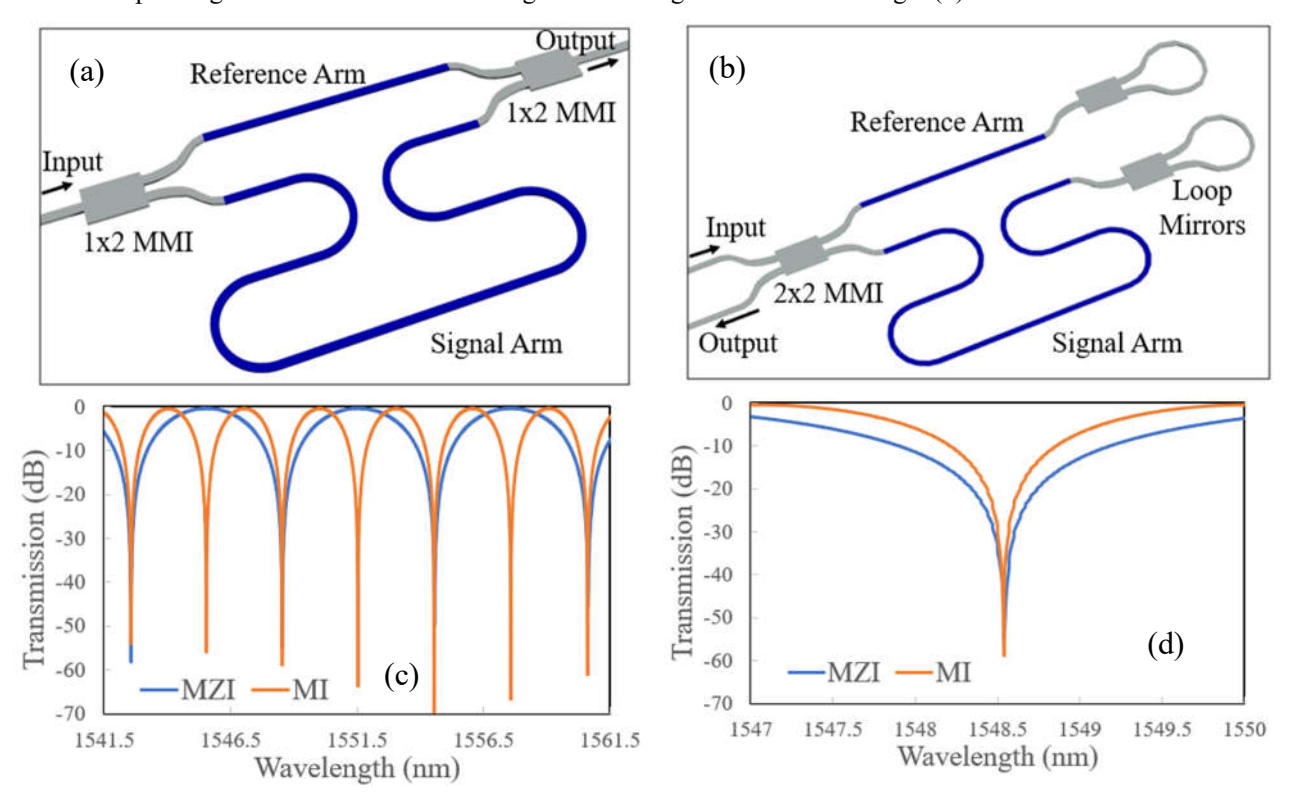


Figure 1. Schematic representation of a silicon photonic (a) Mach-Zehnder interferometer and (b) Michelson Interferometer. (c) Interference fringes observed at the output of the MZI in (a) and the MI in (b) showing twice phase shift with the same geometric path length difference for the MI. (d) Selected interference fringe showing the higher quality factor of the MI compared to the MZI.

The interference fringes in Fig. 1 were achieved for an asymmetric MZI and an asymmetric MI with the same geometric path length difference 100 $\mu$ m between the signal and reference arms. Slow light photonic crystal waveguides (PCWs) have been demonstrated in recent years in the literature in one-dimensional (1-D) and two-dimensional (2-D) periodic structures where group index (ng) ~100 have been experimentally demonstrated. Losses in photonic crystal waveguides tend to scale approximately as group index squared (ng²). Fig. 2 shows a schematic of a Michelson Interferometer with slow wave enhanced 1-D PCWs of different lengths in the two arms in asymmetric MI configuration. As observed in Fig. 2, by assuming a conservative value for the operating group index ng~20, which is approximately 5× the group index in a regular strip waveguides in 220nm silicon clad in silicon dioxide, the effective geometric path length that achieves the same fringe spacing is reduced by a factor of 20/4=5. In Fig. 2, by considering slow light propagation at ng~20 in both arms, the geometric path length difference is reduced to 20 $\mu$ m. Fig. 2 considers PCW lengths 10 $\mu$ m and 30 $\mu$ m in the reference and signal arms respectively. The PCWs need to be designed with appropriate group index adiabatic tapering to maximize the coupling efficiency from the access strip waveguides to the PCWs.

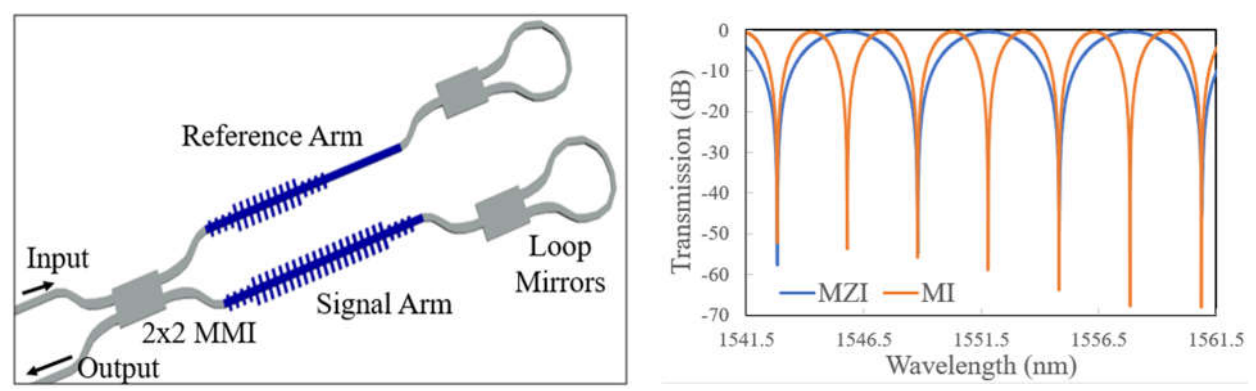


Figure 2. (a) Schematic representation of a silicon photonic Michelson Interferometer with slow wave enhanced 1-D photonic crystal waveguides of different lengths on the signal and reference arms. (b) Interference fringes observed at the output of a MI in (a) and a corresponding MZI formed with the same signal and reference arms in (a) showing twice phase shift with the same geometric path length difference for the MI. (assuming a constant group index profile across the displayed bandwidth)

For the design of asymmetric MIs, we note that the reference arm is covered with silicon dioxide so that it does not come in contact with the analyte liquid. The signal arm is a 1-D PCW in silicon with a top cladding of water. Fig. 3 shows the dispersion diagrams of the 1-D PCWs with an oxide top cladding and a water top cladding respectively. The individual PCWs are designed with lattice constants so as to observe the interferometric behavior in our wavelength range of interest.

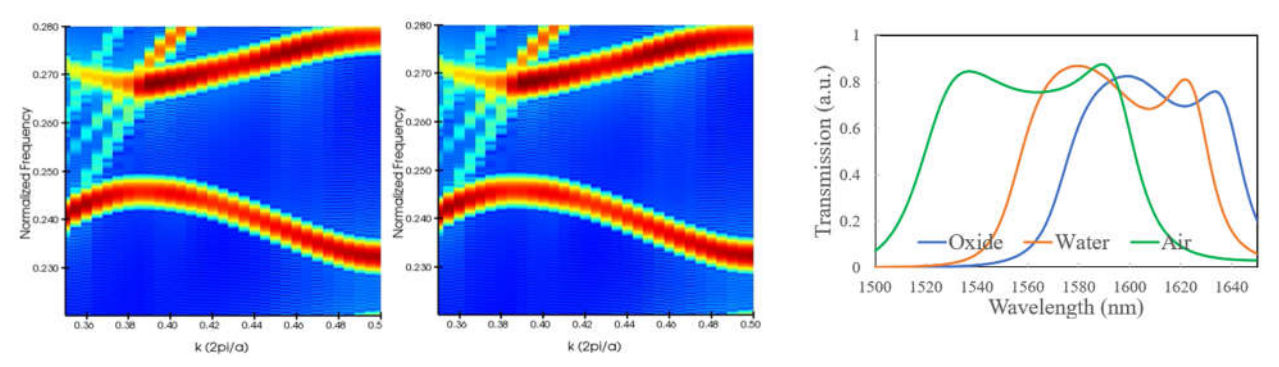
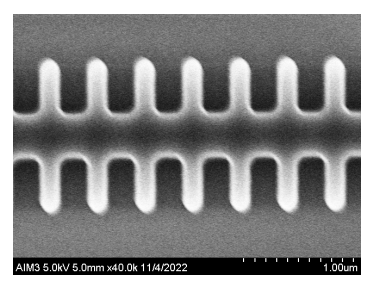


Figure 3. Dispersion diagram of the designed 1-D photonic crystal waveguide with (a) top oxide cladding (refractive index  $n\sim1.45$ ) for the reference arm and (b) top water cladding ( $n\sim1.333$ ) for the signal arm. Devices are designed at the normalized frequency  $a/\lambda\sim0.245$ . (c) 3D finite difference time domain (FDTD) simulated transmission spectrum of a representative 1-D PCW device with period a=370nm and different top cladding, silicon dioxide, water and air respectively. Silicon fins of width 500nm on either side of a central silicon waveguide of width 400nm are arranged with a 40% duty cycle. Four (4) periods of step taper with fins of width 250nm are designed for coupling into the 1-D PCW from a strip waveguide.

Slow light 1-D PCW fishbone structures were designed with lattice constant a=370nm. The width of the central fishbone was w=400nm while the fin length and duty cycle was chosen as 500nm and 40% respectively. In Fig. 2(b), we have assumed that the group index remains constant across a wide bandwidth. While constant group index wide bandwidth designs have been demonstrated experimentally in 2-D PCW structures, such demonstrations have not been achieved in the case of 1-D PCWs without addition of significant additional structures on either side of the device demonstrated in Fig. 2(a). In 1-D PCWs, the transmission spectrum is characterized by a stop band and a slow light high group index propagation region near the band edge over a limited bandwidth of few tens of nanometers in wavelength followed by the lower group index propagation further away from the band edge.

### 3. RESULTS

Fig. 4 shows scanning electron micrographs (SEMs) of fabricated 1-D PCW devices showing the step tapering from strip waveguides to the 1-D PCW in Fig. 4(b).



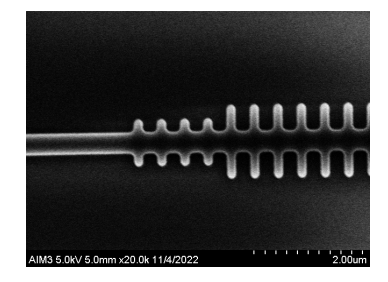


Figure 4. Scanning electron micrographs showing (a) 1-D photonic crystal waveguide and (b) step taper from the strip waveguide to the photonic crystal waveguide.

Fig. 5 shows the transmission spectrum of the reference oxide clad 1-D photonic crystal waveguide showing the transmission band edge around  $\lambda$ ~1562nm. The interference fringes observed at the output of the Michelson interferometer with an air clad signal waveguide are shown in Fig. 5(b). Further measurements are in progress with top water cladding on the signal arm.

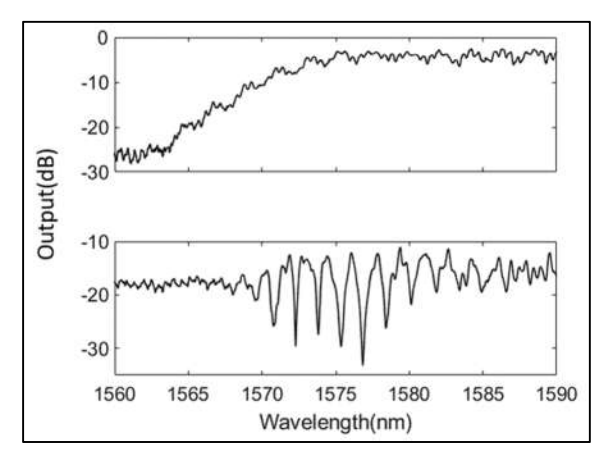


Figure 5. (a) Transmission spectrum of 1-D oxide clad photonic crystal waveguide. (b) Output interference fringes with the reference waveguide clad in oxide and the signal waveguide clad in air.

The maxima and minima of the oscillations correspond to constructive and destructive interference, respectively. The relative phase shift between two adjacent extrema is equal to  $\pi$ . The spectral dependence of the group index in the signal arm can be deduced from positions of corresponding minima  $\lambda_{min}$  and maxima  $\lambda_{max}$  as:

$$n_g^{sig}(\lambda) = \frac{\lambda_{min}\lambda_{max}}{\left[2L[\lambda_{min} - \lambda_{max}]\right]} + n_g^{ref}(\lambda)$$

Where L=20 $\mu$ m×2 = 40 $\mu$ m is the length of the signal 1D-PCW traversed by the optical mode, which evaluates to  $n_g \sim 36$  at  $\lambda \sim 1575$ nm following the method given in ref. [10]

# 4. CONCLUSION

We designed an integrated photonic slow light enhanced Michelson Interferometer (MI) sensor which is able to achieve twice the optical path difference and hence twice the phase shift for refractive index changes in contrast to a Mach-Zehnder interferometer (MZI) with the same geometric path difference. In addition, we have shown that slow light effects in a one-dimensional periodic photonic crystal waveguide can achieve an additional 5× reduction in the geometric path length of the signal arm, for a total of 10× reduction in the geometric path difference to achieve the same optical path difference compared to a strip waveguide based MZI. Preliminary fabricated devices showed interference fringes at the output of the MI. Further measurements are in progress to establish the sensing principle using the shift of the interference fringes.

#### 5. ACKNOWLEDGEMENTS

The research was supported by the National Science Foundation (NSF) under grant #2210707. D.D. acknowledges support from the University of Dayton Summer Undergraduate Research Experience (SURE) program.

# 6. REFERENCE

- [1] Lee, M., and Fauchet, P. M., "Two-dimensional silicon photonic crystal based biosensing platform for protein detection", Opt. Express 15 (8), 4530 (2007)
- [2] Galleogos, D., et al, "Label-free biodetection using a smartphone", Lab-on-a-Chip 13(11), 2124 (2013)
- [3] Iqbal, M., et al., "Labe-free biosensor arrays based on silicon ring resonators and high-speed optical scanning instrumentation", IEEE J. Se. Top. Quant. Electron. 16 (3), 654 (2010)
- [4] Flueckiger, J., et al, "Sub-wavelength grating for enhanced ring resonator biosensor", Opt. Express 24 (14), 15672 (2016)
- [5] Schmitt, K., et al., "Interferometric biosensor based on planar optical waveguide sensor chips for label-free detection of surface bound bioreactions", Biosens. Bioelectron. 22, 2591 (2007)
- [6] Goodwin, M. S., et al, "Highly sensitive protein detection by asymmetric Mach-Zehnder interferometry for biosensing applications", ACS Appl. Bio. Mater. 3 (7), 4566 (2020)
- [7] Chakravarty, S., et al., "Multiplexed Specific Label-Free Detection of NCI-H358 Lung Cancer Cell Line Lysates with Silicon Based Photonic Crystal Microcavity Biosensors", Biosens. Bioelectron. 43, 50 (2013)
- [8] Yan, H., et al, "High-sensitivity high-throughput chip-based biosensor array for multiplexed detection of heavy metals", Proc. of the SPIE 9725, 972507 (2016)
- [9] Chakravarty, S., et al., "Analysis of ultra-high sensitivity configuration in chip-integrated photonic crystal microcavity bio-sensors," Appl. Phys. Lett. 104, 191109 (2014)
- [10] Vlasov, Y. A., et al, "Active control of slow light on a chip with photonic crystal waveguides", Nature 438, 65 (2005)